Osteoarthritis and Cartilage 18 (2010) 539–546

Osteoarthritis and Cartilage

Assessing degeneration of human articular cartilage with ultra-short echo time (UTE) T_2* mapping

A. Williams †, Y. Qian ‡, D. Bear †, C.R. Chu †*

† Cartilage Restoration Laboratory, Department of Orthopaedic Surgery, University of Pittsburgh, Pittsburgh, PA, United States
‡ MR Research Center, Department of Radiology, University of Pittsburgh, Pittsburgh, PA, United States

ARTICLE INFO

Article history:
Received 27 July 2009
Accepted 1 February 2010

Keywords:
Ultra-short TE, UTE
Cartilage
MRI
T_2* mapping
T_2 mapping
Osteoarthritis

SUMMARY

Objective: To examine the sensitivity of ultra-short echo time (UTE) T_2* mapping to collagen matrix degeneration in human articular cartilage.
Methods: Magnetic resonance imaging (MRI) UTE-T_2* maps and standard T_2 maps were acquired on four human tibial plateau explants. Thirty-three osteochondral cores were harvested for polarized light microscopy (PLM), and composition analyses. Collagen matrix integrity was evaluated from PLM and histological images. Matrix integrity and composition was compared to standard T_2 values and UTE-T_2* values on a spatially registered basis.
Results: UTE-T_2* values varied with matrix degeneration ($P = 0.008$) and were lower in severely degraded cartilage compared to healthy tissue ($P = 0.012$). A trend for higher UTE-T_2* values in healthy tissue compared to mildly degenerate tissue ($P = 0.051$) was detected. Standard T_2 values were not found to vary with matrix degeneration ($P = 0.13$) but tended to be higher in severely degraded cartilage compared to healthy tissue. UTE-T_2* value variations were independent of type-II collagen and glycosaminoglycan contents. UTE-T_2* mapping of deep cartilage, adjacent to subchondral bone, was more robust than standard T_2 mapping in this zone.
Conclusion: UTE-T_2* mapping of articular cartilage is sensitive to matrix degeneration and detects short-T_2 signal, particularly in deep tissue, that is not well captured by standard T_2 mapping. Correlation of UTE-T_2* values and PLM indices supports the hypothesis that both may be sensitive to collagen microstructure. Further exploration of UTE-T_2* mapping as a non-invasive tool to detect early articular cartilage degeneration is warranted.

Introduction

As the incidence of osteoarthritis continues to increase, there is a tremendous need for non-destructive diagnosis and staging of cartilage degeneration prior to the onset of irreversible changes[1,2]. Standard clinical imaging modalities used to diagnose articular chondrosis may not be sensitive to subtle articular matrix alterations which occur in the early stages of degeneration[3–5]. Ultra-short echo time (UTE) T_2* mapping is an emerging imaging technology with the potential to detect early degenerative changes in cartilage appearing grossly intact upon visual inspection.

Although magnetic resonance imaging (MRI) has proven to be essential in the diagnosis of articular joint diseases, standard MRI sequences have limited sensitivity to changes in the deep and calcified zones where highly organized collagen fibrils contribute to the very short T_2 relaxation found there and where increased stresses in the tissue lead to early matrix deterioration[6–11]. UTE-T_2* mapping, in which T_2* values are calculated pixel-by-pixel from a series of MRI images with varying echo times (TEs) including an TE of ~0.5 ms or shorter, is sensitive to changes in short-T_2 signal ($T_2 < 10$ ms) and to intravoxel dephasing from local field inhomogeneities[9,12–14]. UTE imaging (TE ~ 0.5 ms or shorter) seeks to minimize short-T_2 signal decay and thus to reveal short-T_2 contrast in tissues where the macromolecular structure restricts proton mobility and causes rapid T_2 relaxation.

UTE imaging of the anisotropic collagen matrix found throughout articular cartilage and particularly in the deep layers may provide an improved sensitivity to subtle matrix alterations that are not well captured by long TE (>10 ms) sequences[7,9,15]. Previously, UTE imaging has been shown to delineate articular cartilage lesions better than gradient echo and magnetization transfer sequences[15]. A recent spectroscopic UTE imaging (UTESI)

* Address correspondence and reprint requests to: Constance R. Chu, Cartilage Restoration Center, 3471 Fifth Ave, Suite 911, Pittsburgh, PA 15213, United States. Tel: 1-412-605-3245; Fax: 1-412-648-8548.
E-mail address: chucr@upmc.edu (C.R. Chu).

1063-4584/$ – see front matter
doi:10.1016/j.joca.2010.02.001

study estimated T_2^* values in deep and calcified cartilage to be between 1 and 2 ms[7].

Polarized light microscopy (PLM) exploits the optical properties of materials to reveal information about their composition and structure. Birefringence, the optical property of anisotropically oriented macromolecules to alter the plane of polarized light, is found in the superficial and deep zones of healthy cartilage where collagen fibrils are highly oriented[16,17]. Loss of birefringence as assessed by PLM has been seen following collagenase-induced matrix disruption[18].

The ability to detect early degeneration, when potentially reversible changes are occurring, could lead to early institution of treatment to prevent or delay the onset of osteoarthritis. Therefore, the aim of this study is to examine the sensitivity of UTE-T_2^* mapping to collagen matrix degeneration in human articular cartilage. We hypothesize that UTE-T_2^* maps will discriminate between normal and abnormal collagen architecture as observed by PLM.

Materials and methods

Sample preparation

Thirty-three osteochondral cores were harvested from four human tibial plateaus. Tibial plateaus were collected from intact cadaveric specimens ($n = 3$; 18-year-old male; 76-year-old male; elderly female, age unknown) and from total knee replacement (TKR) surgery ($n = 1$, 77-year-old female). Tissue samples were obtained in accordance to protocols approved by the Committee for the Oversight of Research for the Dead (CORID) and the Institutional Review Board (IRB).

Tibial plateau explants were dissected and mounted to an acrylic adapter plate using quick-set epoxy. Prior to MRI scans, a registration plate with MRI lucent fiducial markers was rigidly fixed to the acrylic adapter plate with nylon screws. A pattern of precisely located wells filled with 4% agar doped with 2 mM Gd-DTPA^{2-} (Magnevist, Berlex Imaging, Wayne, New Jersey) embedded in the registration plate served as an external reference frame for spatially matching small regions of interest (ROI) on MR images to tissues removed as osteochondral cores (Fig. 1).

Osteochondral core preparation

Following MRI scans osteochondral cores were removed from the tibial plateau explants and processed for histologic and matrix composition evaluation. Two orthogonal linear translation stages with manually driven actuators permitting 1 μm positioning sensitivity and a laser position marker were used to locate tissue regions on the explants. The center of each tissue region to be removed was marked with an India ink pen. Osteochondral cores were removed using an 8.5 mm diameter coring device (Smith & Nephew). Thirty-three osteochondral cores were removed from the tibial plateau explants: six from each explant including two from the submeniscal region, and one from the central region of each medial and lateral compartment, respectively. Due to the larger size of the male explants, additional cores were successfully harvested from the 18-year male ($n = 7$ additional cores) and the 76-year male ($n = 2$ additional cores). Core locations were chosen to coincide with MRI sections that showed good UTE-T_2^*-curve fits, cartilage thick enough to permit ROI segmentation, and encompassing a wide range of UTE-T_2^* values. Cores removed from the TKR explant were harvested in the same manner as cores from the cadaveric specimens. Areas of denuded bone on the TKR explant were excluded from coring. Core locations relative to the registration plate markers were determined to permit spatial registration of MRI, PLM, and composition evaluations. Unique MRI, PLM, and compositional measurements were computed for each osteochondral core.

Quantitative MRI methods

All MR images were collected on a 3 T clinical scanner (MAGNETOM Trio Tim, Siemens Medical Solutions, Erlangen, Germany) using an 8 channel knee coil (Invivo Inc., Gainesville, Florida, USA). Tibial plateau explants were oriented in the bore so that the articular surface was parallel to the main magnetic field (B_0). Acquisition of axially oriented images (relative to the magnet bore) produced coronal cross-sections (relative to the tibial plateau). This orientation served to minimize magic angle effects in the UTE-T_2^* maps as the primary orientation of the collagen fibrils was perpendicular to B_0.

Free induction decay (FID) images for UTE-T_2^* mapping were acquired using a home-developed, fast, three-dimensional (3D), UTE sequence (Acquisition-Weighted Stack of Spirals, AWSOS). A detailed description of the AWSOS sequence has previously been published[14]. Briefly, AWSOS utilizes a hard radio frequency (RF) pulse to excite the entire cartilage explant. The explant is then partitioned into thin slices using variable-duration phase encodings to minimize TE and signal decay caused by short-T_2 relaxation. Spiral trajectories are used for fast in-plane data acquisitions with high spatial resolution. The k-space data collection starts immediately (except 0.04 ms delay for hardware safety) after the slice encoding gradient and the FID signal is encoded by spiral gradients. There is no spin-/gradient-echo used and no contrast agents needed. Total scan time is defined by the product of slice number, in-plane spiral-interleaf number and repetition time (TR).

For UTE-T_2^* mapping in this study on explants, FID images were acquired using a hard RF pulse of duration 0.4 ms at eleven TEs ranging from 0.5 to 40 ms to cover both short- and long-T_2^* relaxations. Fifty slices were collected across a 100 mm field of view (FOV) with a 256×256 matrix for 391×391 μm in-plane resolution and 2 mm section thickness. Sixty-four spiral interleaves were applied with readout time = 5.28 ms, TR = 80 ms, and flip angle (FA) = 30°. Scan time was 4.27 min per TE image and 50 min for all 11-TE images. Fat saturation was achieved by using the scanner's standard fat-saturation blocks (VB15 platform on Tim Trio 3 T, Siemens, Erlangen, Germany) to suppress all fat signals in the explants.

For standard T_2 mapping, a multi-contrast spin echo sequence (se_mc, VB15, Siemens, Erlangen, Germany) was used to acquire multislice coronal 2D images with seven echoes ranging from 10 to 80 ms, and TR = 1800 ms at bandwidth 326 Hz/pix. Twenty slices were collected with 417×417 μm in-plane resolution and 2 mm section thickness. Chemical shift artifact was 1.3 pixels. Total standard T_2 scan time was 12 min.

Standard T_2 maps and UTE-T_2^* maps were generated on a pixel-by-pixel basis with a mono-exponential fitting routine using MRIMapper software (© Beth Israel Deaconess and MIT 2006). Full-thickness cartilage ROI were manually segmented, 10–13 pixels wide by full tissue depth. The ROIs were also further subdivided into superficial and deep halves of equal thickness. Mean UTE-T_2^* and standard T_2 values were calculated for each full-thickness, superficial and deep ROI by averaging across all pixel values within the ROI. ROI locations were determined relative to registration plate fiducial markers and were sized and positioned to correspond to regions of tissue removed during osteochondral coring.

Histology and extracellular matrix composition

Following MR imaging, osteochondral cores were harvested and bisected. One half of each core was processed for matrix

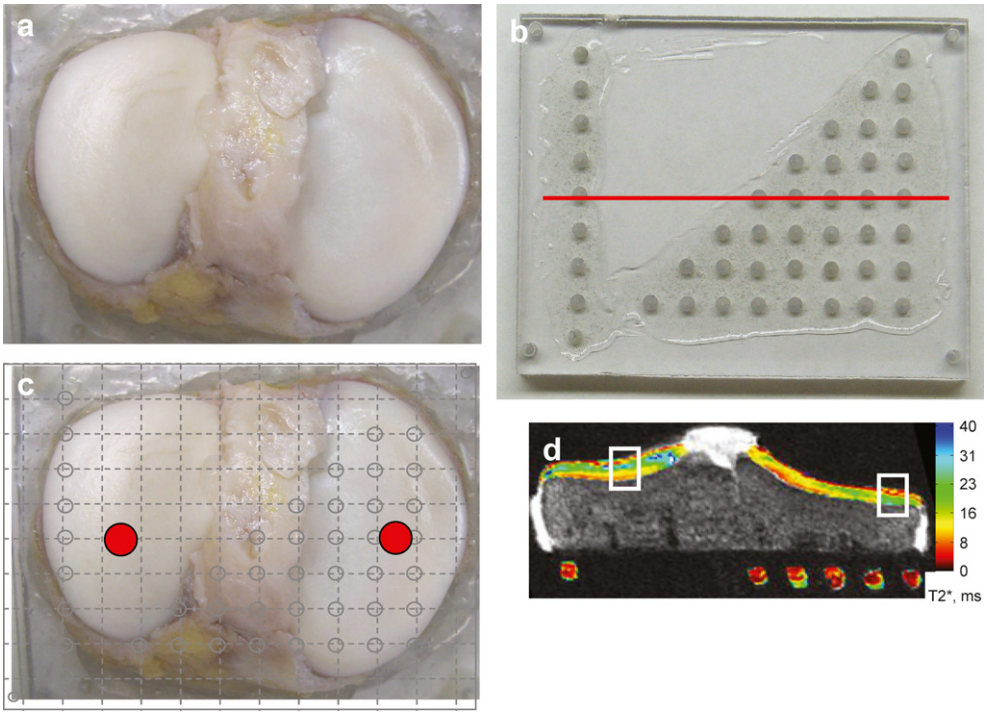

Fig. 1. Spatial registration of MRI and PLM measurements was achieved by (a) mounting the human tibial plateau explants to acrylic adapter plates, and fixing the adapter plates to a 'registration' plate (b) embedded with precisely located MRI lucent markers. Osteochondral core locations (c, red circles) and MRI ROIs (d, white boxes) were spatially matched using the pattern of MRI lucent markers as a common reference frame (b, c, grey circles; d, multi-colored circles). The red line (b) indicates the plane of the example UTE-T_2* map (d).

composition assessment; the other half was processed for histologic assessment. For composition analysis, half-cores were further bisected, and the dry-weight of each quarter-core was determined. Osteochondral quarter-cores were air-dried at room temperature under a tissue-culture hood and massed daily. The sample dry-weight was taken as the mass of the quarter-core when the daily mass ceased to change within the sensitivity of the scale (approximately 0.001 g).

Glycosaminoglycan (GAG) content was determined for one quarter of each osteochondral core by placing the sample in 0.5 M NaOH at 4°C for 48 h. GAG extracts were diluted (1:175 saline), assayed (dimethy-methylene blue)[19], and GAG contents normalized by corresponding dry-weights. Type-II collagen content was determined for the remaining quarter of each osteochondral core by freezing the tissue in liquid nitrogen, crushing the frozen sample to form a powder, then incubating the powder in pepsin (10 ng/ml dissolved in 0.05 M acetic acid) at 4°C for 48 h. Pepsin incubations were repeated a total of three times, then pancreatic elastase was added to the solution (1 mg/ml dissolved in tris buffered saline) at 4°C for 12 h. Extracts were further diluted as needed (between 1:25 and 1:200 in saline), assayed with ELISA (MD Biosciences), and type-II collagen contents normalized by corresponding dry-weights[20]. Each normalized GAG and type-II collagen measurement was further standardized to the average measurement per plateau to allow relative compositions to be compared across multiple tibial plateaus.

For histology, core halves were decalcified (Surgipath Decalcifier I, Surgipath Medical, Richmond, IL), fixed, processed, paraffin-embedded, vertically sectioned and stained with hematoxylin/eosin (HE) and picrosirius red (PSR) using standard techniques[21]. Hemi-cores were sectioned in the coronal plane, parallel to coronal MRI slices. Coronal sectioning orientation was achieved by making a mark on each core at the 12 o'clock position (aligned with the anterior/posterior axis of the plateau, where the 12 o'clock pointed posteriorly). Histologic sections were then sliced orthogonally to the anterior/posterior axis. Histologic sections were approximately 6 μm thick.

PLM analysis of the collagen network was performed using a Nikon Eclipse TE2000-U polarized light microscope (Nikon, Chiyoda-ku, Tokyo) with the two polarizers set orthogonally to each other. PSR stained sections were placed between the polarizers and rotated in the x–y plane of the stage so that the polarizers were arranged 45° against the tissue superficial zone. PLM images were recorded and digitized with an Olympus DP-71 camera and Olympus DP2-BSW software (Olympus, Center Valley, PA).

PLM cross-polarized light transmission analysis

PLM images were saved as 8-bit grayscale images and depthwise cross-polarized light transmission profiles were created by averaging pixel intensities parallel to the cartilage surface (ImageJ, NIH, USA). To compare cross-polarized light transmission profiles across tissue samples with different tissue thicknesses, profiles were plotted against normalized tissue depth where 0 represented the tissue surface and 1 represented the bone/cartilage interface (Matlab, TheMathWorks, Natick, MA).

Qualitative cartilage matrix evaluation

HE and PLM images were qualitatively assessed in accordance with a scale developed by David-Vaudey *et al*[22]. Table I describes histologic and birefringence characteristics and the corresponding matrix grade of the David-Vaudey (DV) scale.

Statistical analyses

Osteochondral cores ($n = 33$) constitute the unit of analysis for this study. Unique values for UTE-T_2*, standard T_2, DV matrix grade,

Table I
DV matrix grading scale. Matrix grading scale based on histologic and PLM characteristics to evaluate the progression of osteoarthritis, developed by David-Vaudey *et al.*[22]

Grade	Histologic characteristics	PLM characteristics
0	No surface irregularities	Presence of birefringence in the surface and deep zone
1	Mild surface fibrillation	Minor disruption of birefringence in the surface
2	Significant surface fibrillation	Disruption of birefringence in the superficial zone
3	Significant surface degeneration and moderate transitional zone degeneration	Complete breakdown of superficial birefringence
4	Significant structural degeneration extending well into the radial zone	Breakdown of birefringence in the superficial as well as deep zone

PLM profile, type-II collagen content and GAG content were calculated for each osteochondral core. The distributions of study metrics were examined both graphically and statistically (*via* Shapiro–Wilk tests) prior to statistical testing and the results indicated that assumptions of normally distributed data were met. Full-thickness UTE-T_2* ROI means and full-thickness standard T_2 ROI means were binned according to DV matrix grade. Mean UTE-T_2* and standard T_2 values, ±standard error of the mean (SEM), for each cartilage matrix grade were calculated. In order to account for the degree of dependency between different cores harvested from the same explant, a mixed model analysis in which the explants were treated as random effects and the DV matrix grades were treated as fixed effects was employed to assess if the full-thickness UTE-T_2* or standard T_2 values varied with DV matrix grade. *Post hoc* tests were performed with Bonferroni adjustment for multiple comparisons to compare the mean full-thickness UTE-T_2* and full-thickness standard T_2 values between samples with different degrees of matrix degeneration. Pearson correlation coefficients were used to test for correlation between type-II collagen and GAG contents and full-thickness UTE-T_2* values. A mixed model analysis was also used to assess the variation of type-II collagen and GAG contents with DV matrix grades. All statistical analyses were performed using Excel (Microsoft, Seattle, WA) and SPSS (SPSS Inc, Chicago, IL). Statistical significance was accepted for $P < 0.05$.

Results

UTE-T_2* map appearances vary with collagen matrix organization; areas of cartilage damage tend to exhibit relatively low UTE-T_2* values (Fig. 2). The deep cartilage adjacent to bone that is poorly detected on the standard T_2 maps has comparatively strong UTE-T_2* signal and typically low UTE-T_2* values. Considerably more noise in the T_2-decay curves was noticed in the deep tissue regions of standard T_2 maps, compared to the curves on the UTE-T_2* maps. For many voxels, a standard T_2 value could not be determined within the tolerances of the curve-fit algorithm [Fig. 2(g, h, i)].

PLM

Depthwise PLM cross-polarized light transmission profiles varied greatly between tissue samples. Of the 33 osteochondral cores examined in this study, only seven cores (four from the 18-year-old male; two from the elderly female; one from the 76-year-old male) demonstrated a cross-polarized light transmission profile typical of intact healthy cartilage with relatively high signal intensity observed both in the superficial and deep zones. Each of these seven osteochondral cores was harvested from the submeniscal region of the plateau (four medial, three lateral) and each was graded as healthy or mildly degenerate (DV matrix grade 0 or 1). None of the cores from the TKR explant exhibited normal profiles. Among the 26 osteochondral cores with cross-polarized light transmission profiles not typical of healthy cartilage, the matrices were found, on average, to exhibit more degeneration (average DV matrix grade = 2.3 ± 1.6). Figure 3 depicts depthwise cross-polarized light transmission profiles corresponding to the three tissue samples shown in Fig. 2.

UTE-T_2 values and standard T_2 values vs DV matrix grading*

The UTE-T_2* value of one core from the TKR knee with DV grade 4 could not be evaluated due to poor signal-to-noise ratio in that region of the image. Across the remaining 32 cores from the four explants, UTE-T_2* values measured in full-thickness ROIs were found to differ with DV matrix grade (mixed model analysis, $F = 4.87$, $P = 0.008$, $n = 32$), with the mean UTE-T_2* value appearing to decrease with increasing matrix degeneration [Fig. 4(a)]. Standard T_2 values were not found to differ significantly with DV matrix grade (mixed model analysis, $F = 5.06$, $P = 0.13$, $n = 33$), although the mean standard T_2 value appeared to increase with increasing matrix degeneration for DV matrix grades 0–3 [Fig. 4(b)]. *Post hoc* analysis with Bonferroni adjustment for multiple comparisons to determine pairwise differences between DV matrix grades for UTE-T_2* indicated that UTE-T_2* values in severely degenerate tissue (DV matrix grade 4, $n = 8$) were lower than UTE-T_2* values of healthy tissue (DV matrix grade 0, $n = 9$; estimated marginal mean difference (EMMD) = −9.3 ms, $P = 0.012$, 95% confidence interval (CI): −17.0 to −1.6). *Post hoc* analysis also detected a trend for lower UTE-T_2* values in mildly degenerate tissue (DV matrix grade 1, $n = 10$) compared to healthy tissue (DV matrix grade 0, $n = 9$; EMMD = −5.9 ms, $P = 0.051$, 95% CI: −11.8 to 0.2).

Matrix composition

Composition assessments did not detect correlations between either type-II collagen or GAG contents and UTE-T_2* values (Pearson's $r = 0.12$, $P = 0.52$, 95% CI: −0.45 to 0.24; Pearson's $r = 0.08$, $P = 0.68$, 95% CI:−0.42 to 0.29, respectively, $n = 31$). Type-II collagen was not found to vary with matrix organization assessed by DV matrix grade (mixed model analysis $F = 1.49$, $P = 0.26$, $n = 27$). GAG content, however, was found to vary with matrix organization (mixed model analysis $F = 3.86$, $P = 0.024$, $n = 27$). *Post hoc* analysis with Bonferroni adjustment for multiple comparisons indicated that the GAG content of moderately degenerate tissue (DV matrix grade 3, $n = 5$) was higher than the GAG content of healthy tissue (DV matrix grade 0, $n = 9$; EMMD = 0.52, $P = 0.018$, 95% CI: 0.07 to 0.97).

Discussion

UTE-T_2* mapping of articular cartilage is sensitive to the degree of organization (and disorganization) in the extracellular matrix and detects short-T_2 signal, particularly in deep tissue, that is not well captured by standard T_2 mapping. In this work, variations in the UTE-T_2* values could not be explained by differences in type-II collagen content suggesting that UTE-T_2* mapping is sensitive to matrix architecture rather than composition.

A purpose of this study was to ascertain whether or not UTE-T_2* values differentiated between healthy and degenerate cartilage in a way consistent with existing metrics (histology, PLM analysis,

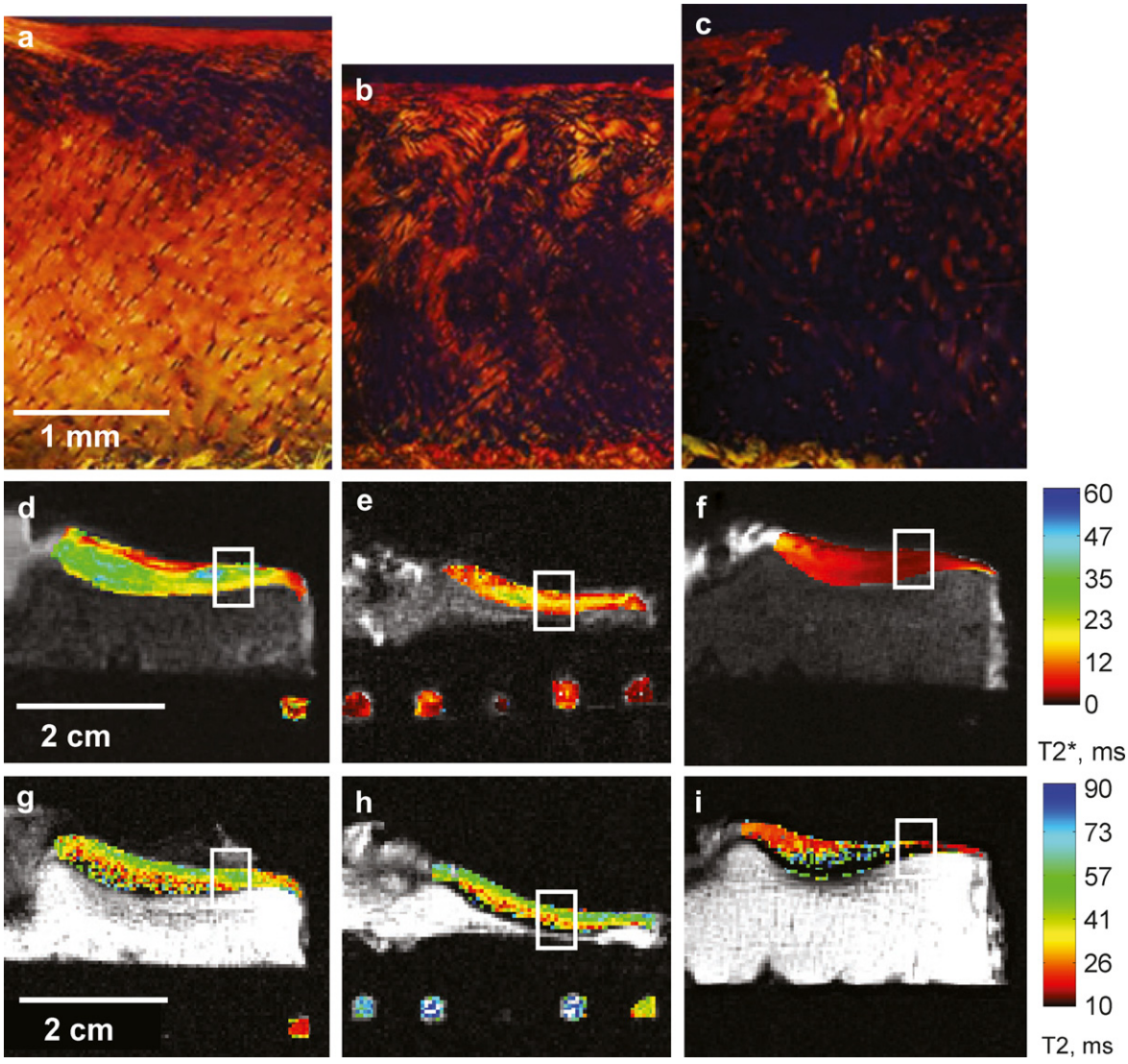

Fig. 2. Example PLM, UTE-T_2*, and standard T_2 maps of human articular cartilage from tibial plateau explants. Low signal adjacent to the bone-cartilage interface in standard T_2 maps (bottom row) prevents robust calculation of standard T_2 in the deepest layers of cartilage. UTE-T_2* maps (middle row) of this region reflect an abundance of short-T_2 components in the deep tissue. (a) The PLM image of healthy cartilage from an 18-year-old male shows an organized matrix with three distinct zones: a bright and intact superficial zone at the surface, a dark middle zone and a thick and bright deep zone extending to bone. UTE-T_2* values in this tissue (d) are relatively high, ranging from 20 to 30 ms. (b) Tissue recovered from TKR surgery exhibits a disorganized matrix beneath an intact articular surface with mid-range UTE-T_2* values (e) around 13 ms. (c) Tissue from a 76-year-old male shows articular fibrillation, lack of deep tissue birefringence and very low UTE-T_2* values (*f*) around 3 ms. White boxes outline tissue regions corresponding osteochondral cores sectioned for histologic and composition analyses. MRI lucent fiducial markers in the registration plate can be seen beneath the tissue in d, e, g, h.

standard T_2 mapping). Beyond confirming that UTE-T_2* values do indeed discriminate between healthy and severely degenerate tissue, the data suggest several benefits of UTE-T_2* mapping over existing technologies: (1) UTE-T_2* mapping is capable of evaluating the deep zone of cartilage which is difficult to examine by other existing non-invasive quantitative methods, and (2) UTE-T_2* shows greater potential than standard T_2 for detecting mild degeneration (UTE-T_2* nearly discriminated healthy from mildly diseased tissue, $P = 0.051$). Although the ability of UTE-T_2* mapping to detect the earliest stages of disease (matrix alterations prior to the breakdown of the articular surface) remains to be established, the finding that UTE-T_2* values varied with PLM-based matrix evaluation of the tissue warrants further exploration of UTE-T_2* mapping as a non-invasive tool to detect early degeneration.

The ultra short echo times collected in this study permitted the influence of short-T_2 components (<10 ms) on the T_2* measurement. Short-T_2 components, from fast spin-spin interactions between bound and free water molecules, arise in cartilage tissue where free water closely associates with protons bound in the collagen fibrils[12]. A higher concentration of constrained collagen fibrils in the highly anisotropic deep and calcified zones of cartilage gives rise to shorter T_2 times in deep tissue compared to the middle zone[8,10]. Standard T_2 sequences, with typical echo times of 10 ms or longer, are insensitive to short-T_2 signals that decay more rapidly than they can be measured. The UTE-T_2* values measured in this study reflect signal from both long and short-T_2 components of cartilage tissue, therefore, UTE-T_2* mapping has a wider sensitivity to cartilage degeneration than standard T_2 mapping.

In contrast to the widely recognized tendency for standard T_2 values to increase with matrix damage[28,31–33], UTE-T_2* values measured in this study were found to *decrease* with increasing matrix degeneration. The reason for this behavior can not be conclusively determined from this study. However, it may be speculated that a loss of water trapped within collagen fibrils

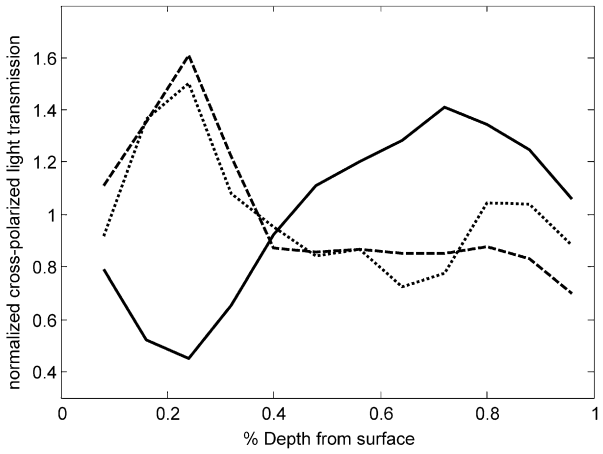

Fig. 3. Example cross-polarized light transmission intensity profiles corresponding to samples shown in Fig. 2. In order to compare profiles across samples, the intensities are presented as normalized by the mean intensity for the sample. The solid line, from the tissue shown in Fig. 2(a), demonstrates a cross-polarized light transmission profile typically seen in healthy tissue where collagen fibril anisotropy creates birefringence in the superficial and deep zones. The decrease of light transmission in the middle zone shows a more randomly organized matrix. The dotted and dashed profiles correspond to tissues from Fig. 2(b, c), respectively. These two samples exhibit a relative lack of birefringence in the deep half of tissue indicative of a chaotic collagen matrix structure.

($T_2 \sim 4$ ms)[23] may result in a relative increase of shorter T_2 component intensities in the measured FID decay curve thus leading to a net decrease in UTE-T_2* value which includes contributions from all measured T_2 components. In standard T_2 mapping, by contrast, a loss of trapped water increases the dominance of long-T_2 components on the T_2-decay curve resulting in a larger standard T_2 value. Loss of trapped water may occur in early disease and/or in deep tissue, if the extracellular matrix becomes loosened or damaged.

Standard T_2 maps poorly detected signal from the deepest layer of cartilage adjacent to bone. In fact, the standard T_2 data in deep tissue was so noisy that a T_2 value could not be determined within the tolerances of the curve-fit algorithm for many voxels. Interpretation of the standard T_2 values that were measured in this study is complicated by the fact that T_2 is known to be sensitive to both collagen network integrity and tissue hydration[24]. Collagen network disruption has been shown to reduce T_2[25], while fragmentation of the network accompanied by an increase in hydration, has been shown to increase T_2[22,26–28]. Since changes to matrix structure and hydration produce competing effects on the T_2 parameter, and since both are altered with degeneration, it is difficult to determine cartilage status on the basis of standard T_2 alone.

In the current study, special hardware and protocols were employed to spatially match tissue regions and section orientations across imaging modalities. By employing a common reference using MR lucent markers on the registration plate, micrometer driven actuators with 1 μm positioning resolution and laser-guided core location and orientation tracking, the expected spatial registration error between PLM and MRI evaluations in this work is within 2 mm (the thickness of an MRI section). However, the disparity in image scales between the assessment modalities (PLM images are micrometers thick and MRI image are millimeters thick) mean that different quantities of tissue were represented by each measurement. Additionally, the DV matrix evaluation was available only for the actual plane of histologic sectioning. Although the plane corresponding to the MR scan was marked for histological section, it remains possible that the collagen microstructure assessed by the DV matrix grade differed from the macrostructural arrangement assessed by MRI either due to slight mismatch in plane of section or due to the disparity in image scale. Furthermore, the PLM analysis scheme employed in this work did not attempt to measure total birefringence. Rather, it used birefringence intensity within the superficial and deep zones (observed in a single plane, in a single histologic slice, at a single orientation with respect to the polarizers) as a proxy for gross collagen organization[22]. Despite these limitations, the quantitative spatial agreement between MRI and PLM indices suggests that UTE-T_2* mapping is sensitive to collagen matrix architecture.

Degenerative articular cartilage disease is known to manifest with extensive regional variation across the tibial plateau[29–33]. In the current work, however, variation in the study metrics is due to a combination of disease-dependant variation and inter-individual variations. Although inter-individual variations could not be effectively assessed due to the small number of tibial plateau explants examined, mixed model analyses were used to account for dependencies between samples harvested from the same explant. After considering the dependency imposed by multiple cores from the same explants, UTE-T_2* was still found to vary with the degree of matrix degeneration. Given that previous *in vitro* cartilage research has examined multiple samples from the same subject without explicit acknowledgment of such limitations[34–36], the field would benefit from appropriate usage of mixed model statistical analyses in the future. Regarding this study, the degree to which inter-individual UTE-T_2* variations depend on disease or injury-induced tissue degeneration relative to inherent variations between healthy individuals requires further examination.

The results of this study showed that UTE-T_2* mapping was sensitive to changes in the sub-surface matrix microstructure of articular cartilage. UTE-T_2* was found to be more robust than

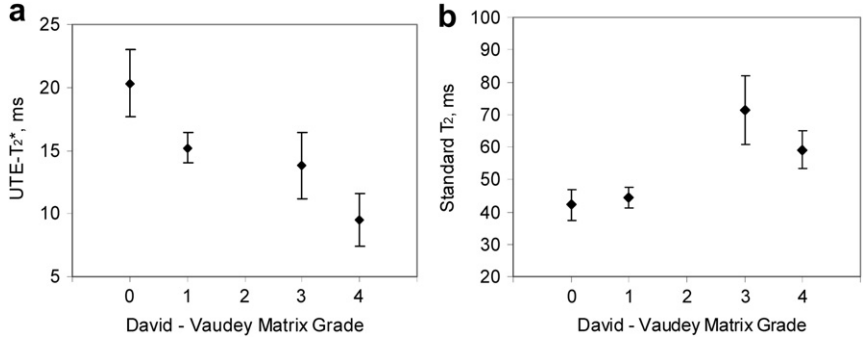

Fig. 4. UTE-T_2* values and standard T_2 values vary in opposite directions with matrix organization. Matrix organization is measured according to the DV matrix grading scale shown in Table I. (a) UTE-T_2* values decrease with increasing matrix degeneration, ($P = 0.008$, $n = 32$). The UTE-T_2* value of tissue with DV matrix grade 0 is 40% higher than DV matrix grade 4 tissue, ($P = 0.012$, $n = 9.8$, respectively). (b) Although standard T_2 values were not found to vary significantly with matrix degeneration ($P = 0.13$, $n = 33$), they tended to increase with increasing degeneration. None of the tissue samples examined were assigned a grade 2 by the DV matrix grading scale. Error bars represent ±S.E.M.

standard T_2 mapping in detecting the deepest layers of cartilage. This study demonstrates a new and promising non-invasive technique for imaging articular cartilage matrix structure which may permit improved diagnosis of articular degeneration.

Conflict of interest

The authors of this work, Assessing degeneration of human articular cartilage with ultra-short echo time (UTE) T_2^* mapping, have no financial or personal relationships to disclose that may constitute a conflict of interest.

Acknowledgement

The authors gratefully acknowledge the National Institutes of Health for providing funding for this work (NIH RO1 AR052784, AR052784-03S1), and the generous statistical analysis assistance by Dr James Irrgang.

References

1. Helmick CG, Felson DT, Lawrence RC, Gabriel S, Hirsch R, Kwoh CK, *et al*. Estimates of the prevalence of arthritis and other rheumatic conditions in the United States. Part I. Arthritis Rheum 2008 Jan;58(1):15–25.
2. Lawrence RC, Helmick CG, Arnett FC, Deyo RA, Felson DT, Giannini EH, *et al*. Estimates of the prevalence of arthritis and selected musculoskeletal disorders in the United States. Arthritis Rheum 1998 May;41(5):778–99.
3. Recht M, Bobic V, Burstein D, Disler D, Gold G, Gray M, *et al*. Magnetic resonance imaging of articular cartilage. Clin Orthop Relat Res 2001 Oct;391(Suppl):S379–96.
4. Disler DG, McCauley TR, Kelman CG, Fuchs MD, Ratner LM, Wirth CR, *et al*. Fat-suppressed three-dimensional spoiled gradient-echo MR imaging of hyaline cartilage defects in the knee: comparison with standard MR imaging and arthroscopy. AJR Am J Roentgenol 1996 Jul;167(1):127–32.
5. Buckland-Wright JC. Quantitative radiography of osteoarthritis. Ann Rheum Dis 1994 Apr;53(4):268–75.
6. Burr DB. Anatomy and physiology of the mineralized tissues: role in the pathogenesis of osteoarthrosis. Osteoarthritis Cartilage 2004;12(Suppl A):S20–30.
7. Du J, Takahashi AM, Chung CB. Ultrashort TE spectroscopic imaging (UTESI): application to the imaging of short T2 relaxation tissues in the musculoskeletal system. J Magn Reson Imaging 2009 Feb;29(2):412–21.
8. Freeman DM, Bergman G, Glover G. Short TE MR microscopy: accurate measurement and zonal differentiation of normal hyaline cartilage. Magn Reson Med 1997 Jul;38(1):72–81.
9. Robson MD, Bydder GM. Clinical ultrashort echo time imaging of bone and other connective tissues. NMR Biomed 2006 Nov;19(7):765–80.
10. Xia Y, Farquhar T, Burton-Wurster N, Ray E, Jelinski LW. Diffusion and relaxation mapping of cartilage-bone plugs and excised disks using microscopic magnetic resonance imaging. Magn Reson Med 1994 Mar;31(3):273–82.
11. McCauley TR, Recht MP, Disler DG. Clinical imaging of articular cartilage in the knee. Semin Musculoskelet Radiol 2001 Dec;5(4):293–304.
12. Gatehouse PD, Bydder GM. Magnetic resonance imaging of short T2 components in tissue. Clin Radiol 2003 Jan;58(1):1–19.
13. Gatehouse PD, Thomas RW, Robson MD, Hamilton G, Herlihy AH, Bydder GM. Magnetic resonance imaging of the knee with ultrashort TE pulse sequences. Magn Reson Imaging 2004 Oct;22(8):1061–7.
14. Qian Y, Boada FE. Acquisition-weighted stack of spirals for fast high-resolution three-dimensional ultra-short echo time MR imaging. Magn Reson Med 2008 Jul;60(1):135–45.
15. Brossmann J, Frank LR, Pauly JM, Boutin RD, Pedowitz RA, Haghighi P, *et al*. Short echo time projection reconstruction MR imaging of cartilage: comparison with fat-suppressed spoiled GRASS and magnetization transfer contrast MR imaging. Radiology 1997 May;203(2):501–7.
16. Goodwin DW, Dunn JF. High-resolution magnetic resonance imaging of articular cartilage: correlation with histology and pathology. Top Magn Reson Imaging 1998 Dec;9(6):337–47.
17. Nieminen MT, Rieppo J, Toyras J, Hakumaki JM, Silvennoinen J, Hyttinen MM, *et al*. T2 relaxation reveals spatial collagen architecture in articular cartilage: a comparative quantitative MRI and polarized light microscopic study. Magn Reson Med 2001 Sep;46(3):487–93.
18. Nieminen MT, Toyras J, Rieppo J, Hakumaki JM, Silvennoinen J, Helminen HJ, *et al*. Quantitative MR microscopy of enzymatically degraded articular cartilage. Magn Reson Med 2000 May;43(5):676–81.
19. Mort JS, Roughley PJ. Measurement of glycosaminoglycan release from cartilage explants. Methods Mol Med 2007;135: 201–9.
20. Rennard SI, Berg R, Martin GR, Foidart JM, Robey PG. Enzyme-linked immunoassay (ELISA) for connective tissue components. Anal Biochem 1980 May 1;104(1):205–14.
21. Junquiera LC, Junqueira LC, Brentani RR. A simple and sensitive method for the quantitative estimation of collagen. Anal Biochem 1979 Apr 1;94(1):96–9.
22. David-Vaudey E, Ghosh S, Ries M, Majumdar S. T2 relaxation time measurements in osteoarthritis. Magn Reson Imaging 2004 Jun;22(5):673–82.
23. Lattanzio PJ, Marshall KW, Damyanovich AZ, Peemoeller H. Macromolecule and water magnetization exchange modeling in articular cartilage. Magn Reson Med 2000 Dec;44(6):840–51.
24. Mosher TJ, Dardzinski BJ. Cartilage MRI T2 relaxation time mapping: overview and applications. Semin Musculoskelet Radiol 2004 Dec;8(4):355–68.
25. Menezes NM, Gray ML, Hartke JR, Burstein D. T2 and T1rho MRI in articular cartilage systems. Magn Reson Med 2004 Mar;51(3):503–9.
26. Dunn TC, Lu Y, Jin H, Ries MD, Majumdar S. T2 relaxation time of cartilage at MR imaging: comparison with severity of knee osteoarthritis. Radiology 2004 Aug;232(2):592–8.
27. Mosher TJ, Dardzinski BJ, Smith MB. Human articular cartilage: influence of aging and early symptomatic degeneration on the spatial variation of T2 – preliminary findings at 3 T. Radiology 2000 Jan;214(1):259–66.
28. Stahl R, Blumenkrantz G, Carballido-Gamio J, Zhao S, Munoz T, Hellio Le Graverand-Gastineau MP, *et al*. MRI-derived T2 relaxation times and cartilage morphometry of the tibio-femoral joint in subjects with and without osteoarthritis during a 1-year follow-up. Osteoarthritis Cartilage 2007 Nov;15(11):1225–34.
29. Bear DM, Williams A, Chu CT, Coyle CH, Chu CR. Optical coherence tomography grading correlates with MRI T2 mapping and extracellular matrix content. J Orthop Res 2009 Oct 15.
30. Chu CR, Izzo NJ, Irrgang JJ, Ferretti M, Studer RK. Clinical diagnosis of potentially treatable early articular cartilage degeneration using optical coherence tomography. J Biomed Opt 2007 Sep–Oct;12(5):051703.
31. Hannila I, Susanna Raina S, Tervonen O, Ojala R, Nieminen MT. Topographical variation of T2 relaxation time in the young adult knee cartilage at 1.5T. Osteoarthritis Cartilage 2009;12:1570–5.
32. Mosher TJ, Smith H, Dardzinski BJ, Schmithorst VJ, Smith MB. MR imaging and T2 mapping of femoral cartilage: in vivo

determination of the magic angle effect. AJR Am J Roentgenol 2001 Sep;177(3):665–9.
33. Samosky JT, Burstein D, Eric Grimson W, Howe R, Martin S, Gray ML. Spatially-localized correlation of dGEMRIC-measured GAG distribution and mechanical stiffness in the human tibial plateau. J Orthop Res. 2005 Jan;23(1):93–101.
34. Froimson MI, Ratcliffe A, Gardner TR, Mow VC. Differences in patellofemoral joint cartilage material properties and their significance to the etiology of cartilage surface fibrillation. Osteoarthritis Cartilage 1997 Nov;5(6):377–86.
35. Gillis A, Gray M, Burstein D. Relaxivity and diffusion of gadolinium agents in cartilage. Magn Reson Med 2002 Dec;48(6):1068–71.
36. Wheaton AJ, Casey FL, Gougoutas AJ, Dodge GR, Borthakur A, Lonner JH, *et al*. Correlation of T1rho with fixed charge density in cartilage. J Magn Reson Imaging 2004 Sep;20(3):519–25.